A hypoxia-responsive albumin-based nanosystem for deep tumor penetration and excellent therapeutic efficacy

Yang, Guangbao; Phua, Fiona Soo Zeng; Lim, Wei Qi; Zhang, Rui; Feng, Liangzhu; Liu, Guofeng; Wu, Hongwei; Bindra, Anivind Kaur; Jana, Deblin; Liu, Zhuang; Zhao, Yanli

2019

Yang, G., Phua, F. S. Z., Lim, W. Q., Zhang, R., Feng, L., Liu, G., ... Zhao, Y. (2019). A hypoxia-responsive albumin-based nanosystem for deep tumor penetration and excellent therapeutic efficacy. Advanced Materials, 31(25), 1901513-. doi:10.1002/adma.201901513

https://hdl.handle.net/10356/137689

https://doi.org/10.1002/adma.201901513

DOI: 10.1002/((please add manuscript number))

Article type: Communication

Hypoxia-responsive albumin-based nanosystem for deep tumor penetration and excellent therapeutic efficacy

Guangbao Yang[1], Soo Zeng Fiona Phua[1], Wei Qi Lim[1], Rui Zhang[2], Liangzhu Feng[2], Guofeng Liu[1], Hongwei Wu[1], Anivind Kaur Bindra[1], Deblin Jana[1], Zhuang Liu[2], Yanli Zhao[1]**

Dr. G. Yang, S. Z. F. Phua, W.Q. Lim, Dr. G. Liu, Dr. H. Wu, A. K. Bindra, D. Jana, Prof. Y. L. Zhao

Division of Chemistry and Biological Chemistry, School of Physical and Mathematical Sciences, Nanyang Technological University, 21 Nanyang Link, 637371, Singapore.

*E-mail: zhaoyanli@ntu.edu.sg

R. Zhang, Dr. L. Feng, Prof. Z. Liu

Institute of Functional Nano & Soft Materials (FUNSOM), Jiangsu Key Laboratory for Carbon-Based Functional Materials & Devices, Soochow University, 199 Ren'ai Road, Suzhou, 215123, Jiangsu, China.

*E-mail: zliu@suda.edu.cn

Abstract

Uncontrolled cancer cell proliferation, insufficient blood flow, and inadequate endogenous oxygen lead to hypoxia in the tumor tissues. Herein, we report a unique type of hypoxia-responsive human serum albumin (HSA)-based nanosystem (HCHOA) prepared by cross-linking hypoxia-sensitive azobenzene group between photosensitizer chlorin e6 (Ce6)-conjugated HSA (HC) and oxaliplatin prodrug-conjugated HSA (HO). The HCHOA nanosystem is stable under normal oxygen partial pressure with the size of 100-150 nm. When exposed to hypoxic tumor microenvironment, the nanosystem could quickly dissociate into ultrasmall HC and HO therapeutic nanoparticles with the diameter smaller than 10 nm, significantly enabling their enhanced intratumoral penetration. After the dissociation, the quenched fluorescence of Ce6 in the produced HC nanoparticles could be recovered for bioimaging. At the same time, the production of singlet oxygen was increased because of the enhancement in the photoactivity of the photosensitizer. On account of these improvements, the combined photodynamic therapy and chemotherapy were realized to display superior antitumor efficacy *in vivo*. Based on this simple strategy, we were able to achieve the dissociation of

hypoxic-responsive nanosystem to enhance the tumor penetration and therapeutic effect.

Keywords: chemotherapy, human serum albumin, hypoxia, intratumoral penetration, photodynamic therapy

Versatile nanoparticles for precise delivery of therapeutic drugs to solid tumors show a great prospect to enhance the treatment efficiency and reduce systemic side effects during the administration.[1] On account of the malformation of blood vessels and dense extracellular matrix in the tumor microenvironment, nanoparticles must overcome the barriers of interstitial delivery to achieve deep tumor penetration.[2] The size of nanoparticles plays an important role in transporting them to deep tumor tissues, since the diffusion distance is inversely proportional to the particle size.[3] Nanoparticles with larger sizes of approximately 100-150 nm, although possessing a great advantage in improving pharmacokinetics and prolonging the blood circulation, are inferior in the case of tumor penetration due to their large diffusion barrier in the tumor space as compared to their ultrasmall counterpart.[4] On the contrary, nanoparticles with ultrasmall sizes below 10 nm have better tumor penetration capability but shorter blood circulation half-life and ineffective tumor accumulation because of their rapid clearance.[5] Ideally, nanoparticles should have relatively larger diameters to achieve better tumor accumulation by enhanced permeability and retention (EPR) effect during the blood circulation, and could release therapeutic ultrasmall nanoparticles that are loaded or attached to the large nanoparticles upon arrival at the tumor site.[6]

Size-switchable therapeutic nanoagents capable of responsive to external stimuli (*e.g.*, light, radiation, and ultrasound) or intrinsic tumor microenvironment conditions (*e.g.*, pH, redox, and enzyme) have been developed to achieve deeper tumor penetration, better tumor accumulation, and more effective treatment efficiency.[7] Hypoxia, caused by insufficient oxygen supply, is a common feature in most solid tumors.[8] Hypoxic and normoxic tissues show significant differences in the microenvironment, providing an opportunity for tumor-specific diagnosis and treatment triggered by oxygen partial pressure.[9] It has also been reported that azobenzene derivatives could be reduced to aniline derivatives by various reductases and this process is closely related to the degree of hypoxia.[10] Due to excellent hypoxia-sensitive property, azobenzene derivatives have been employed as hypoxia-responsive fluorescent probes to detect hypoxia levels[11] and for the delivery of therapeutic drugs[12] or genes[13] to hypoxic cancer cells. However, azobenzene-based nanoparticles with hypoxia-responsive dissociation capacity to augment the tumor penetration and therapeutic efficiency have still not been well investigated

so far.

Human serum albumin (HSA) as a major component of serum proteins has been widely used for the drug delivery on account of its intrinsic biocompatibility, abundant source and having a variety of functional groups for facile modifications.[14] In this work, we synthesized a size-switchable nanosystem (HCHOA) by using a hypoxia-responsive azobenzene linker to covalently bridge photosensitizer chlorin e6 (Ce6)-conjugated HSA (HC) and oxaliplatin prodrug-conjugated HSA (HO). At normal oxygen partial pressure, the HCHOA nanosystem possesses the diameter of around 100 to 150 nm, beneficial for their long-term blood circulation and enhanced tumor accumulation through the EPR effect. Under hypoxic conditions, these large nanoparticles rapidly dissociate into ultrasmall HC and HO nanoparticles with the diameter below 10 nm owing to the cleavage of the azobenzene moiety in the HCHOA structure by numerous reductases, leading to a significant increase in intratumoral permeability. Upon the dissociation under hypoxic environment, the quenched photoactivity of Ce6 in the HCHOA nanosystem could be activated with enhanced fluorescence and singlet oxygen production for achieving better therapeutic outcome.

The tailored design of the HCHOA nanosystem is showed in **Figure 1a**. The Ce6 photosensitizer and Oxa(IV)-COOH prodrug were separately conjugated with HSA *via* the formation of amide bonds to produce albumin-based ultrasmall HC and HO nanoparticles with the diameter of less than 10 nm (Figure S1), respectively. Then, different amounts of hypoxia-sensitive linker, azobenzene-4,4'-dicarboxylic acid, were added to covalently crosslink HC and HO (1:1 weight ratio) by carbodiimide hydrochloride / N-hydroxysuccinimide coupling, yielding HCHOA assemblies. Under hypoxic conditions, hypoxia-responsive azobenzene moiety in the HCHOA nanosystem would be reduced and cleaved, resulting in the dissociation of the nanosystem into ultrasmall HC and HO therapeutic agents with enhanced penetration into deep tumor tissues for better tumor-inhibiting outcome (Figure 1b,c).

Transmission electron microscopy (TEM) images and dynamic light scattering (DLS) data revealed that the sizes of obtained HCHOA nanoparticles increased from 77.2 nm to 604.6 nm upon increasing the weight ratio of the hypoxia-responsive linker (Figure 1d,e). The size of the products rapidly expanded to be more than 500 nm when the weight ratio exceeded 0.8:10, due to the nanoparticle self-aggregation. As illustrated by UV-Vis spectra (Figure 1f), the absorbance of HCHOA nanoparticles at around 335 nm corresponding to the azobenzene linker was obviously enhanced with the increasing concentration of the added linker, suggesting successful incorporation of gradually rising linker content in the synthesized nanoparticles. On the other hand, the fluorescence of HCHOA nanoparticles gradually decreased upon increasing

the weight ratio of azobenzene linker, which was mainly due to the fluorescence quenching effect of incorporated Ce6 under increased assembly (Figure 1g).[15] As compared with free Ce6, HC showed slightly reduced efficiency of light-induced singlet oxygen generation at the same Ce6 concentration (Figure 1h). Larger HCHOA nanoparticles appeared to produce less singlet oxygen, which may be caused by reducing the photoactivity of photosensitizer.

The HCHOA obtained with the weight ratio of 0.4:10 between the azobenzene linker and HSA protein was employed for further investigations, since the nanoparticles produced in this ratio exhibited the diameter of 100-150 nm suitable for blood circulation and effective tumor passive accumulation.[16] Concomitantly, considering the fact that this particular type of nanoparticles would produce less singlet oxygen than other smaller nanoparticles under normoxic conditions, there was favorable reduction of phototoxicity to normal tissues even when they were illuminated by stray light during animal studies. The loading capacities of Ce6 and Oxa(Ⅳ) in this type of HCHOA were measured using absorbance spectra and inductively coupled plasma optical emission spectrometry (ICP-OES), which were 1.28 % and 1.82 %, respectively.

As an important control, 4’4-biphenyldicaboxylic acid (H_2BPDC) that is stable under hypoxic environment was used to covalently conjugate with HC and HO under the same method, affording the HCHOH nanoparticles. As demonstrated by TEM images and DLS measurements, HCHOH exhibited similar morphology and diameter to HCHOA **(Figure 2a-d)**, suggesting that HCHOH is a suitable system for comparison.

We first studied whether the HCHOA nanoparticles could be stored for a long period of time. After the lyophilization, the HCHOA nanoparticles were instantaneously re-dissolved in phosphate buffered saline (PBS) with no obvious size change (Figure 2f), showing a great storage capacity for future applications. The obtained nanoparticles could also be well dispersed in different solutions, including water, PBS and cell culture medium, without any aggregation after the incubation for 3 days, indicating its excellent stability under physiological conditions (Figure S2). To explore the hypoxia-responsive degradability of these nanoparticles, HCHOH and HCHOA were incubated in simulated hypoxic conditions using rat liver microsomes with nicotinamide adenine dinucleotide phosphate (NADPH) and argon gas bubbling for various treatment periods. The morphology of HCHOH exhibited no significant change after 24 h as shown by the TEM images, suggesting that HCHOH was rather stable in hypoxic conditions (Figure 2e). Interestingly, HCHOA showed time-dependent degradation into ultrasmall species in hypoxic environments on account of the cleavage of the azo bond. These results demonstrate that the azo bond cleavage in HCHOA is directly responsible for the degradation.[17]

For most conventional organic light emitting materials, their luminescence is often weakened or quenched in aggregated state, which is referred to as aggregation-caused quenching (ACQ).[18] Similarly, photochemical efficiency of a photosensitizer drops sharply when its concentration is increased or it is densely encapsulated in nanocarriers, attributed to the ACQ effect and obvious reduction in the generation of reactive oxygen species.[19] Therefore, the fluorescence and singlet oxygen production from photosensitizers would be rapidly enhanced when changing them from aggregated state to free monomeric state.

We hypothesized that the fluorescence and photoactivity of loaded Ce6 would be recovered after the hypoxia-induced degradation of the HCHOA nanoparticles into ultrasmall HC and HO species. Indeed, the fluorescence of Ce6 was significantly enhanced by treating the HCHOA nanoparticles under hypoxic conditions over time (Figure 2g). On the contrary, the fluorescence of Ce6 in HCHOH did not exhibit significant change under hypoxic conditions. In addition to the fluorescence recovery, the singlet oxygen generation capability was tested using singlet oxygen sensor green (SOSG) as an indicator.[20] The photosensitizing ability of these two types of nanoparticles with the same Ce6 concentration was evaluated by comparing their singlet oxygen production efficiency under the 660 nm light irradiation (Figures 2h and S3). Untreated HCHOH and HCHOA nanoparticles displayed similar photosensitizing capabilities as indicated by the similar increase in the SOSG fluorescence. For HCHOH and HCHOA nanoparticles pretreated with rat liver microsomes/NADPH under hypoxic conditions for 24 h, the singlet oxygen generation capacity was significantly enhanced from HCHOA as compared to HCHOH. This phenomenon could be accounted by the hypoxia-triggered generation of ultrasmall therapeutic HC and HO, leading to significant enhancement in the photoactivity of the photosensitizer.[21] These results are consistent with the TEM observations, validating that the azobenzene linker conjugating between HC and HO could be cleaved to recover the fluorescence and consequently the photoactivity of Ce6.

Intracellular hypoxia-responsive degradation of HCHOA was then evaluated *in vitro*. First, the intracellular uptake efficacy of HCHOA nanoparticles by 4T1 murine breast cancer cells was examined by confocal laser scanning microcopy **(Figure 3a)**. Strong Ce6 fluorescence inside cells was observed after prolonging the incubation time, suggesting that HCHOA could be sufficiently internalized by the cells. Next, we studied the *in vitro* cell-killing efficiency of various samples including free Oxa(IV) prodrug, HO, and HCHOA after the incubation with 4T1 cells for 48 h (Figure S4). The obtained data reveal that, although HO and HCHOA were less cytotoxic than free prodrug, they were still sufficiently efficient in killing cancer cells.

To evaluate the PDT efficiency, corresponding nanoparticles without the Oxa(Ⅳ) prodrug,

i.e., HCHA containing the azobenzene linker and HCHH having the H_2BPDC linker were synthesized as controls using HC and untreated HSA (1:1 ratio) under the abovementioned method. Different samples (free Ce6, HC, HCHH and HCHA) were incubated with 4T1 cells under normoxic or hypoxic conditions for 12 h and then irradiated with 660 nm light (20 mW cm^{-2}) for 1 h. After further 24 h incubation, relative cell viability was studied by the standard 3-(4,5-dimethylthiazol-2-yl)-2,5-diphenyltetrazolium bromide (MTT) assay (Figure 3b,c). Both free Ce6 and HC exhibited high phototoxicity to cells in oxygen-rich environment, but significantly weak phototoxicity in hypoxic conditions mainly due to insufficient oxygen supply. As compared to HCHH, light-induced cell destruction efficiency of HCHA remained at higher level even under hypoxic conditions where oxygen level was approximately 1%.

The effect of combinational therapy was then investigated *in vitro* by subjecting the 4T1 cells with HCHA, HCHOH or HCHOA (Figure 3d,e). After the incubation with different samples for 12 h, cells were either kept in the dark or irradiated with 660 nm light for 20 min (20 mW cm^{-2}). As compared to PDT alone (HCHA plus irradiation) and chemotherapy alone (HCHOA in the dark), the combined treatment by HCHOA with light irradiation was found to be most effective in cancer cell killing effect under either normoxic or hypoxic conditions. In contrast, HCHOH could effectively kill tumor cells under normoxic conditions, while the killing effect under hypoxia was significantly weakened. Confocal images of Calcein AM and propidium iodide (PI) stained 4T1 cells after various treatments further validated the cell viability data by the MTT assay (Figure 3f). In comparison to HCHOH nanoparticles, hypoxia-sensitive HCHOA could dissociate into free protein-based therapeutic species under hypoxic conditions, showing enhanced photoactivity of the photosensitizer to promote the PDT performance for enabling combined effect of PDT and chemotherapy.

Tumor-associated fibroblastic cells and extracellular matrix in the tumor microenvironment contain large amounts of collagen and proteoglycans as barriers to obstruct the penetration of large-sized nanoparticles.[22] Due to the presence of hypoxia in the tumor microenvironment, the penetration of HCHOA after the dissociation into free HSA-based complexes should be investigated in detail. It was hypothesized that, under hypoxic environment, the dissociation of larger HCHOA nanoparticles into ultrasmall HC and HO complexes could enhance the penetration into solid tumors. As an *in vitro* model, 3D multicellular tumor spheroids (MCTSs) were utilized to study the penetration behavior by incubating free Ce6, HC, HCHOH, or HCHOA with MCTSs under hypoxic conditions. After the incubation with different formulations for 24 h, the sample penetration within MCTSs was observed by confocal microscopy. As revealed in **Figure 4a**, bright red fluorescence in the case of free Ce6 and HC

was widely distributed in most regions of MCTSs, mainly because of their smaller sizes that enable better penetration. For MCTSs incubated with HCHOH, however, the fluorescence of Ce6 rapidly decreased upon increasing depth and only localized at the peripheral region of these MCTSs, indicating inadequate penetration ability of HCHOH with diameters in the range of 100-150 nm. On the other hand, HCHOA displayed better penetration capability. This is due to its dissociation into ultrasmall HC and HO complexes under hypoxic environment for better penetration, and thus Ce6 fluorescence could be visualized in MCTSs at increased depth as compared to HCHOH.

To observe the intra-tumoral distribution of different formulations, we performed immunofluorescence staining assay for tumor slices obtained from mice injected with HC, HCHOH, or HCHOA nanoparticles (Figure 4b). After intravenous injection of different nanoparticles for 24 h, the tumors were stained with anti-CD31 antibody to visualize blood vessels and then imaged by confocal microscope. For mice injected with HCHOH, the fluorescence of Ce6 was mostly colocalized with or situated near tumor blood vessels, indicating limited tumor penetration of HCHOH nanoparticles. In the tumor slices of mice injected with HC or HCHOA nanoparticles, Ce6 florescence was detected away from blood vessels, confirming outstanding extravascular diffusion ability of HC and HCHOA nanoparticles. These results demonstrate that HCHOA could be degraded into ultrasmall albumin complexes to enable efficient tumor diffusion in hypoxic tumor microenvironment, showing a great potential to enhance the therapeutic effect of tumor.

Next, 4T1 tumor-bearing mice after intravenous injection of different nanoparticles were imaged by Maestro EX optical imaging system for verifying the accumulation of HCHOA (Figure 4c). The fluorescence signal of Ce6 from ultrasmall HC nanoparticles was significantly weakened over time due to rapid clearance by the mouse body. After mice were injected with HCHOH nanoparticles, the fluorescence signal at the tumor region was not obviously observed, because of severe quenching of the Ce6 fluorescence in these nanoparticles with larger size (Figure 4d,e). Interestingly, HCHOA nanoparticles presented higher tumor accumulation visualized by *in vivo* fluorescence, mainly due to the recovery of the Ce6 fluorescence at hypoxic tumor microenvironment after hypoxia-responsive dissociation into ultrasmall complexes. The mice were sacrificed at 24 h after intravenous injection of various nanoparticles, and major organs were harvested. The semi-quantitative biodistribution of these nanoparticles in tumors and major organs further showed that the Ce6 fluorescence of HCHOA nanoparticles in the tumor site was significantly stronger than that of other formulations (Figure 4d,f). In particular, HC nanoparticles exhibited lower fluorescence as compared to HCHOA

nanoparticles, possibly due to poor blood circulation lifetime of such small nanoparticles. In addition, quantitative biodistribution measurements were conducted by measuring the Pt level in different organs using ICP-OES (Figure S5). The results evidenced better tumor uptake of HCHOA nanoparticles through enhanced EPR effect as compared to ultrasmall sized HO nanoparticles after intravenous injection. Furthermore, kidneys in the group of HO nanoparticles showed higher Pt signal, further indicating that the nanoparticles could be rapidly excreted from the body *via* the renal metabolism.

In order to verify that the strategy of using hypoxia-induced nanoparticle dissociation would be useful in improving the efficacy of cancer treatment *in vivo*, thirty nude mice bearing 4T1 tumors were used, including group 1: untreated; group 2: HCHOA; group 3: HCHA plus 660 nm light irradiation; group 4: HCHOH plus 660 nm light irradiation; group 5: HCHOA plus 660 nm light irradiation (Ce6: 4 mg kg^{-1}, Oxa(IV): 5.7 mg kg^{-1}). As shown in **Figure 5a**, the tumor growth was slightly suppressed by chemotherapy with HCHOA (Group 2) or PDT with HCHA (Group 3). Similarly, for mice injected with HCHOH under 660 nm light irradiation (Group 4), the development of tumor was only moderately inhibited. Significantly, it was observed that the group of HCHOA with light irradiation (Group 5) offered the greatest tumor growth inhibition as compared to all other treatment groups. The average tumor weights and corresponding photographs of tumors excised from different treatment groups illustrated that the HCHOA nanoparticles with light irradiation presented the best antitumor efficiency (Figure 5b,c). Therefore, relying on specific microenvironment of tumor hypoxia, HCHOA nanoparticles could be dissociated to ultrasmall albumin-based complexes for deeper penetration into tumor tissues, achieving synergistic effect of enhanced PDT and chemotherapy.

In addition, hematoxylin and eosin (H&E) staining was conducted for tumor slices after various treatments (Figure 5e). The results indicate that the HCHOA nanoparticles with light irradiation led to the highest degree of cancer cell apoptosis as compared with other groups, which is consistent with the obtained therapeutic outcome based on tumor volumes. H&E stained images of major organs from HCHOA treated mice showed that this therapeutic system did not cause any noticeable tissue damage or side effect to these normal organs (Figure S6). The body weight of mice was not affected by various treatments, suggesting that there was no serious systemic toxicity to the mice after the administration of HCHOA nanoparticles (Figure 5d). Furthermore, the serum biochemistry assay and complete blood panel tests were conducted at the same time, showing no significant difference as compared with those of untreated control mice (Table S1). Therefore, these results demonstrated that HCHOA nanoparticles showed no obvious toxicity to mice after 14 days under the tested dosage.

In summary, multifunctional intelligent hypoxia-responsive HCHOA nanoparticles have been successfully developed by a simple covalent cross-linking method for combinational PDT and chemotherapy. The HCHOA nanoparticles with sizes of 100-150 nm upon systemic administration show longer blood circulation and better tumor accumulation than that of control groups. In hypoxic tumors, the azobenzene group in HCHOA nanoparticles would be cleaved by reductases, resulting in the dissociation into individual HC and HO complexes with diameters of below 10 nm to present significantly improved intratumoral penetration as compared to non-hypoxia responsive HCHOH nanoparticles with similar sizes to HCHOA. On account of the dissociation of HCHOA nanoparticles into ultrasmall albumin-based complexes under hypoxic conditions, the photoactivity of Ce6 could be activated to recover its fluorescence and increase the production of singlet oxygen. As a result, great anti-tumor outcome has been achieved on animal models after combined PDT and chemotherapy with HCHOA under light irradiation. Thus, we have designed a simple nanosystem that utilizes the microenvironment of tumor hypoxia to enhance the diffusion of nanoparticles and achieve better therapeutic effect. This work presents an elegant strategy to demonstrate tumor hypoxia-responsive size change of therapeutic agents for enhanced intratumoral penetration and improved anticancer performance. More importantly, albumin-based nanosystem is composed of biocompatible and biodegradable components, which shows enormous potential for future clinical translation.

Supporting Information

Supporting Information is available from the Wiley Online Library or from the author.

Acknowledgements

This research is supported by the Singapore Agency for Science, Technology and Research (A*STAR) AME IRG grant (No. A1883c0005), the Singapore National Research Foundation Investigatorship (No. NRF-NRFI2018-03), Collaborative Innovation Center of Suzhou Nano Science and Technology, and a Project Funded by the Priority Academic Program Development (PAPD) of Jiangsu Higher Education Institutions.

Received: ((will be filled in by the editorial staff))

Revised: ((will be filled in by the editorial staff))

Published online: ((will be filled in by the editorial staff))

References

[1] a) Y. Chen, Q. Meng, M. Wu, S. Wang, P. Xu, H. Chen, Y. Li, L. Zhang, L. Wang, J. Shi, *J. Am. Chem. Soc.* **2014**, *136*, 16326; b) R. de la Rica, D. Aili, M. M. Stevens, *Adv. Drug Delivery Rev.* **2012**, *64*, 967; c) G. Yang, L. Xu, Y. Chao, J. Xu, X. Sun, Y. Wu, R. Peng, Z. Liu, *Nat. Commun.* **2017**, *8*, 902; d) K. Yang, Y. Liu, Y. Liu, Q. Zhang, C. Kong, C. Yi, Z. Zhou, Z. Wang, G. Zhang, Y. Zhang, N. M. Khashab, X. Chen, Z. Nie, *J. Am. Chem. Soc.* **2018**, *140*, 4666.

[2] a) Z. Yang, Q. Chen, J. Chen, Z. Dong, R. Zhang, J. Liu, Z. Liu, *Small* **2018**, 1803262; b) Q. Chen, L. Feng, J. Liu, W. Zhu, Z. Dong, Y. Wu, Z. Liu, *Adv. Mater.* **2016**, *28*, 7129; c) S. Ruan, X. Cao, X. Cun, G. Hu, Y. Zhou, Y. Zhang, L. Lu, Q. He, H. Gao, *Biomaterials* **2015**, *60*, 100.

[3] a) K. Huang, H. Ma, J. Liu, S. Huo, A. Kumar, T. Wei, X. Zhang, S. Jin, Y. Gan, P. C. Wang, S. He, X. Zhang, X.-J. Liang, *ACS Nano* **2012**, *6*, 4483; b) S. Ruan, Q. He, H. Gao, *Nanoscale* **2015**, *7*, 9487.

[4] G. Yang, H. Gong, T. Liu, X. Sun, L. Cheng, Z. Liu, *Biomaterials* **2015**, *60*, 62.

[5] a) S. Zhang, C. Sun, J. Zeng, Q. Sun, G. Wang, Y. Wang, Y. Wu, S. Dou, M. Gao, Z. Li, *Adv. Mater.* **2016**, *28*, 8927; b) Z. Sun, H. Xie, S. Tang, X.-F. Yu, Z. Guo, J. Shao, H. Zhang, H. Huang, H. Wang, P. K. Chu, *Angew. Chem. Int. Ed.* **2015**, *127*, 11688.

[6] a) C. Wong, T. Stylianopoulos, J. Cui, J. Martin, V. P. Chauhan, W. Jiang, Z. Popović, R. K. Jain, M. G. Bawendi, D. Fukumura, *Proc. Natl. Acad. Sci. U.S.A.* **2011**, *108*, 2426; b) Q. Lei, S.-B. Wang, J.-J. Hu, Y.-X. Lin, C.-H. Zhu, L. Rong, X.-Z. Zhang, *ACS Nano* **2017**, *11*, 7201.

[7] a) P. Zhang, J. Wang, H. Chen, L. Zhao, B. Chen, C. Chu, H. Liu, Z. Qin, J. Liu, Y. Tan, X. Chen, G. Liu, *J. Am. Chem. Soc.* **2018**, *140*, 14980; b) H.-J. Li, J.-Z. Du, J. Liu, X.-J. Du, S. Shen, Y.-H. Zhu, X. Wang, X. Ye, S. Nie, J. Wang, *ACS Nano* **2016**, *10*, 6753; c) Y. Niu, J. Zhu, Y. Li, H. Shi, Y. Gong, R. Li, Q. Huo, T. Ma, Y. Liu, *J. Controlled Release* **2018**, *277*, 35.

[8] a) Y. Lou, P. C. McDonald, A. Oloumi, S. K. Chia, C. Ostlund, A. Ahmadi, A. Kyle, U. auf dem Keller, S. Leung, D. G. Huntsman, B. Clarke, B. W. Sutherland, D. Waterhouse, M. B. Bally, C. D. Roskelley, C. M. Overall, A. Minchinton, F. Pacchiano, F. Carta, A. Scozzafava, N. Touisni, J.-Y. Winum, C. T. Supuran, S. Dedhar, *Cancer Res.* **2011**, *71*, 3364; b) R. K. Jain, *Cancer Cell* **2014**, *26*, 605.

[9] a) W. R. Wilson, M. P. Hay, *Nat. Rev. Cancer* **2011**, *11*, 393; b) D.-W. Zheng, B. Li, C.-X. Li, J.-X. Fan, Q. Lei, C. Li, Z. Xu, X.-Z. Zhang, *ACS Nano* **2016**, *10*, 8715.

[10] a) P. Yuan, H. Zhang, L. Qian, X. Mao, S. Du, C. Yu, B. Peng, S. Q. Yao, *Angew. Chem. Int. Ed.* **2017**, *56*, 12481; b) W. Piao, S. Tsuda, Y. Tanaka, S. Maeda, F. Liu, S. Takahashi, Y. Kushida, T. Komatsu, T. Ueno, T. Terai, T. Nakazawa, M. Uchiyama, K. Morokuma, T. Nagano,

K. Hanaoka, *Angew. Chem. Int. Ed.* **2013**, *52*, 13028.

[11] K. Kiyose, K. Hanaoka, D. Oushiki, T. Nakamura, M. Kajimura, M. Suematsu, H. Nishimatsu, T. Yamane, T. Terai, Y. Hirata, T. Nagano, *J. Am. Chem. Soc.* **2010**, *132*, 15846.

[12] a) P. Kulkarni, M. K. Haldar, P. Katti, C. Dawes, S. You, Y. Choi, S. Mallik, *Bioconjugate Chem.* **2016**, *27*, 1830; b) P. Kulkarni, M. K. Haldar, S. You, Y. Choi, S. Mallik, *Biomacromolecules* **2016**, *17*, 2507.

[13] F. Perche, S. Biswas, T. Wang, L. Zhu, V. P. Torchilin, *Angew. Chem. Int. Ed.* **2014**, *126*, 3430.

[14] a) Q. Chen, C. Liang, C. Wang, Z. Liu, *Adv. Mater.* **2015**, *27*, 903; b) Z. Sheng, D. Hu, M. Zheng, P. Zhao, H. Liu, D. Gao, P. Gong, G. Gao, P. Zhang, Y. Ma, L. Cai, *ACS Nano* **2014**, *8*, 12310; c) Y.-R. Zheng, K. Suntharalingam, T. C. Johnstone, H. Yoo, W. Lin, J. G. Brooks, S. J. Lippard, *J. Am. Chem. Soc.* **2014**, *136*, 8790.

[15] M. Noh, T. Kim, H. Lee, C.-K. Kim, S.-W. Joo, K. Lee, *Colloids Surf. A* **2010**, *359*, 39.

[16] X. Duan, Y. Li, *Small* **2013**, *9*, 1521.

[17] C. Huang, J. Zheng, D. Ma, N. Liu, C. Zhu, J. Li, R. Yang, *J. Mater. Chem. B* **2018**, *6*, 6424.

[18] a) W. Z. Yuan, P. Lu, S. Chen, J. W. Y. Lam, Z. Wang, Y. Liu, H. S. Kwok, Y. Ma, B. Z. Tang, *Adv. Mater.* **2010**, *22*, 2159; b) H. He, Y. Xie, Y. Lv, J. Qi, X. Dong, W. Zhao, W. Wu, Y. Lu, *Adv. Healthc. Mater.* **2018**, *7*, 1800711.

[19] M. Li, Y. Gao, Y. Yuan, Y. Wu, Z. Song, B. Z. Tang, B. Liu, Q. C. Zheng, *ACS Nano* **2017**, *11*, 3922.

[20] a) P. Huang, J. Lin, X. Wang, Z. Wang, C. Zhang, M. He, K. Wang, F. Chen, Z. Li, G. Shen, D. Cui, X. Chen, *Adv. Mater.* **2012**, *24*, 5104; b) Y. Cheng, H. Cheng, C. Jiang, X. Qiu, K. Wang, W. Huan, A. Yuan, J. Wu, Y. Hu, *Nat. Commun.* **2015**, *6*, 8785.

[21] Z. Dong, L. Feng, Y. Hao, M. Chen, M. Gao, Y. Chao, H. Zhao, W. Zhu, J. Liu, C. Liang, Q. Zhang, Z. Liu, *J. Am. Chem. Soc.* **2018**, *140*, 2165.

[22] a) K. Kessenbrock, V. Plaks, Z. Werb, *Cell* **2010**, *141*, 52; b) D. Hanahan, L. M. Coussens, *Cancer Cell* **2012**, *21*, 309; c) P. Friedl, S. Alexander, *Cell* **2011**, *147*, 992.

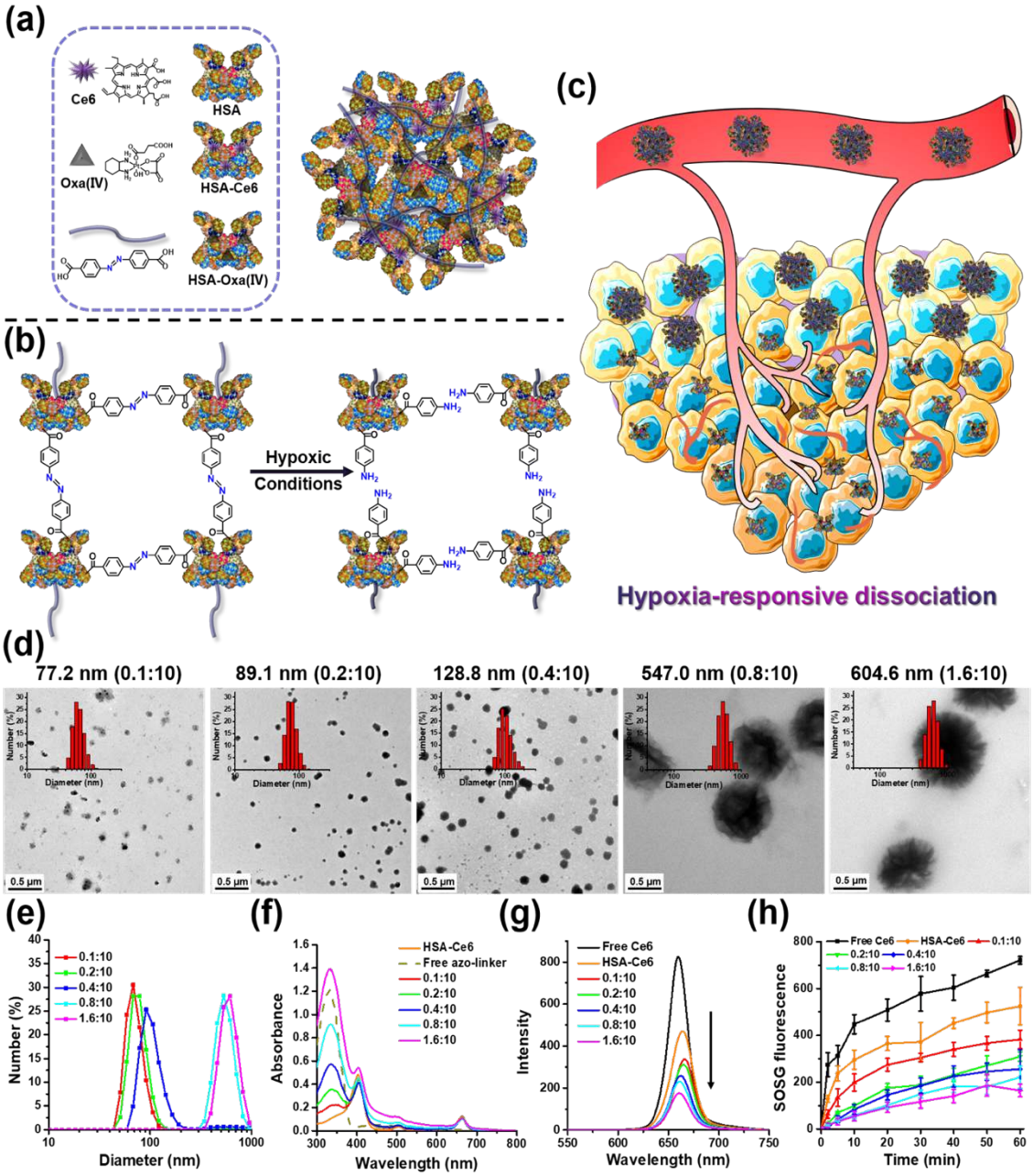

Figure 1. Synthesis and characterization of HCHOA nanoparticles. (a) Schematic illustration about HCHOA and its the components. (b) Scheme indicating hypoxia-responsive dissociation of HCHOA. (c) Scheme showing that, in the microenvironment of tumor hypoxia, hypoxia-responsive HCHOA could disintegrate into individual HSA-based complexes with improved tumor penetrating ability. (d) TEM images of HCHOA with different particle sizes synthesized at different weight ratios of azo-linker and albumin. (e) DLS data of HCHOA with different size prepared under different feeding ratios of azo-linker and albumin. (f) UV-vis-NIR spectra of different HCHOA nanoparticles. (g) Fluorescence intensity of different HCHOA nanoparticles with the same Ce6 concentrations. (h) Production of singlet oxygen measured by the enhanced SOSG fluorescence for free Ce6, HSA-Ce6, and HCHOA nanoparticles with different sizes.

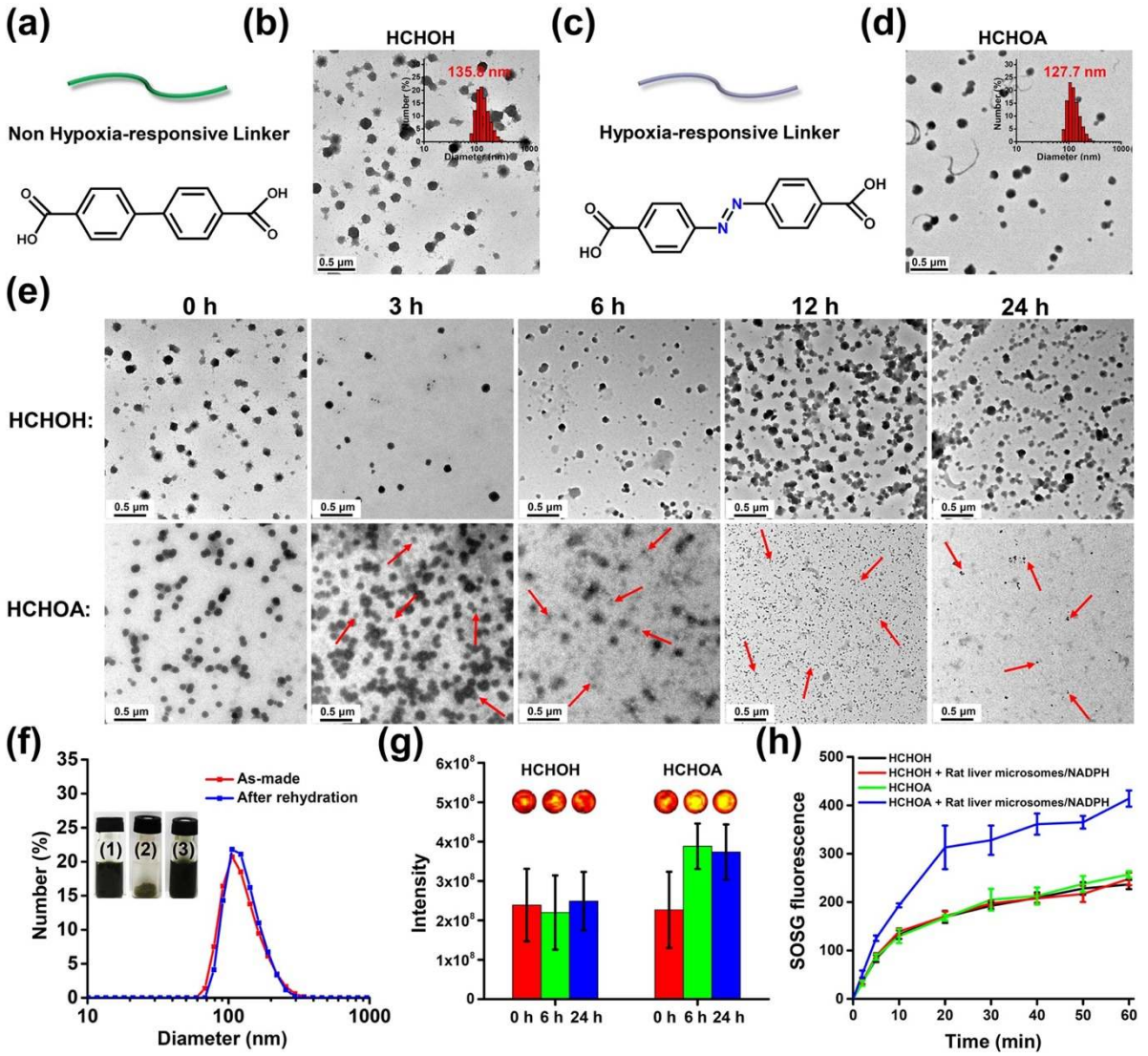

Figure 2. Hypoxia-responsive nanoparticle dissociation. (a) Structure of non-hypoxia-responsive linker and (b) TEM image and DLS data of HCHOH synthesized using linker (a). (c) Structure of hypoxia-responsive azo-linker and (d) TEM image and DLS date of HCHOA synthesized using linker (c). (e) TEM images of HCHOH and HCHOA nanoparticles after incubation with rat liver microsomes/NADPH under hypoxia conditions for various periods of time. (f) DLS size distribution of as-made HCHOA and the rehydrated sample after lyophilization. Insets were the images of HCHOA before (1) lyophilization, (2) after lyophilization, and (3) after rehydration. (g) Time-dependent fluorescence intensity of HCHOH and HCHOA after being incubated with rat liver microsomes/NADPH under hypoxic conditions. Insets were the corresponding fluorescence images of HCHOH and HCHOA after being incubated with rat liver microsomes/NADPH under hypoxic conditions in different time intervals. (h) Production of singlet oxygen measured by the enhanced SOSG fluorescence. The groups of HCHOH and HCHOA treated with rat liver microsomes/NADPH were pre-incubated in hypoxic conditions for 24 h.

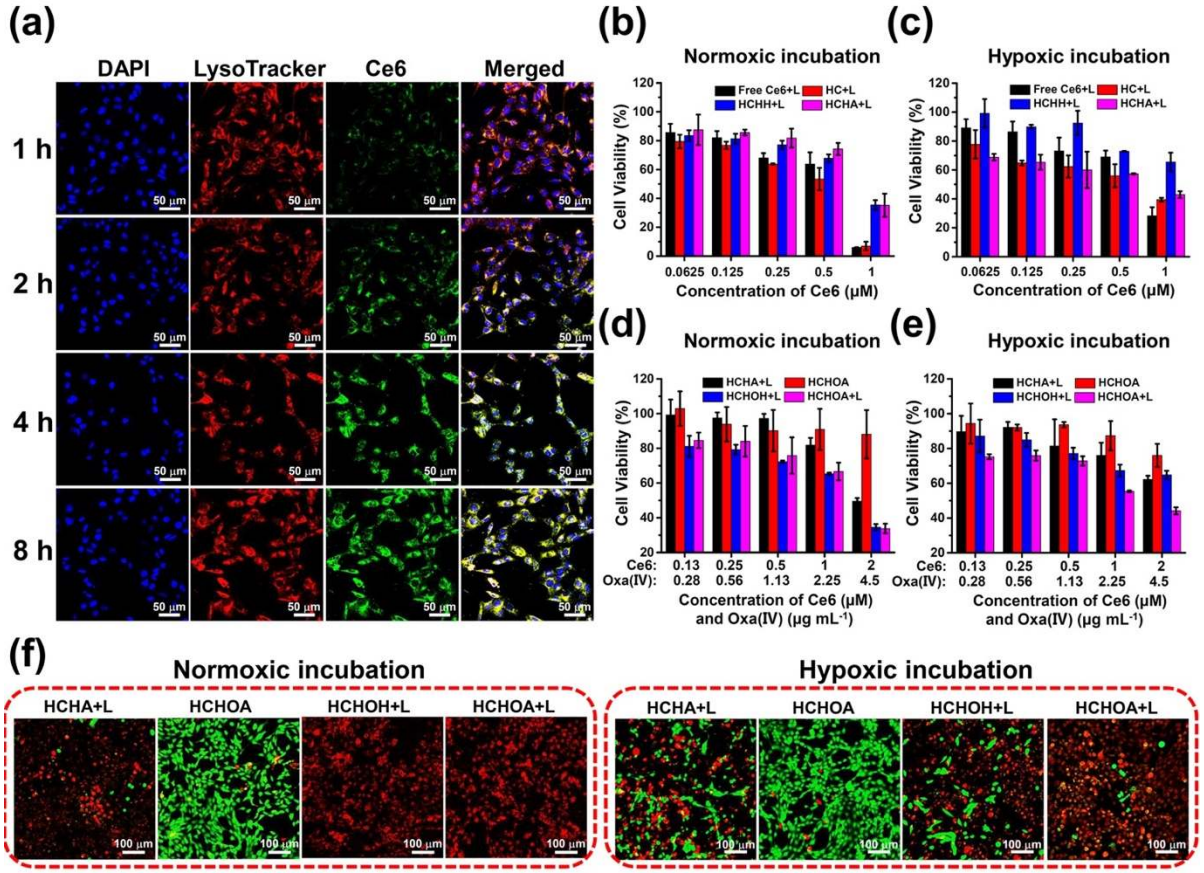

Figure 3. *In vitro* cell culture experiments. (a) Confocal images of HCHOA nanoparticles incubated with 4T1 cells at different time points. Blue, red, and green colors represent 4',6-diamidino-2-phenylindole (DAPI), lysotracker-stained endosomes/lysosomes, and Ce6 fluorescence, respectively. *In vitro* PDT treatment of 4T1 cells by free Ce6, HC, HCHH, or HCHA under 660 nm light irradiation (20 mW cm^{-2}, 1 h) with (b) normoxic or (c) hypoxic incubation (1 % O_2 and 5 % CO_2 balanced with N_2). Relative viability of 4T1 cells after incubation with HCHA plus light irradiation, HCHOH plus light irradiation, and HCHOA with or without light irradiation (660 nm, 20 mW cm^{-2}, 20 min) in (d) normoxic or (e) hypoxic conditions. (f) Confocal fluorescence images of Calcein AM/PI stained 4T1 cells after various treatments in normoxic or hypoxia conditions (Ce6: 4 μM, Oxa(IV): 9 μg mL^{-1}). Green and red colors represent Calcein AM and PI fluorescence, respectively.

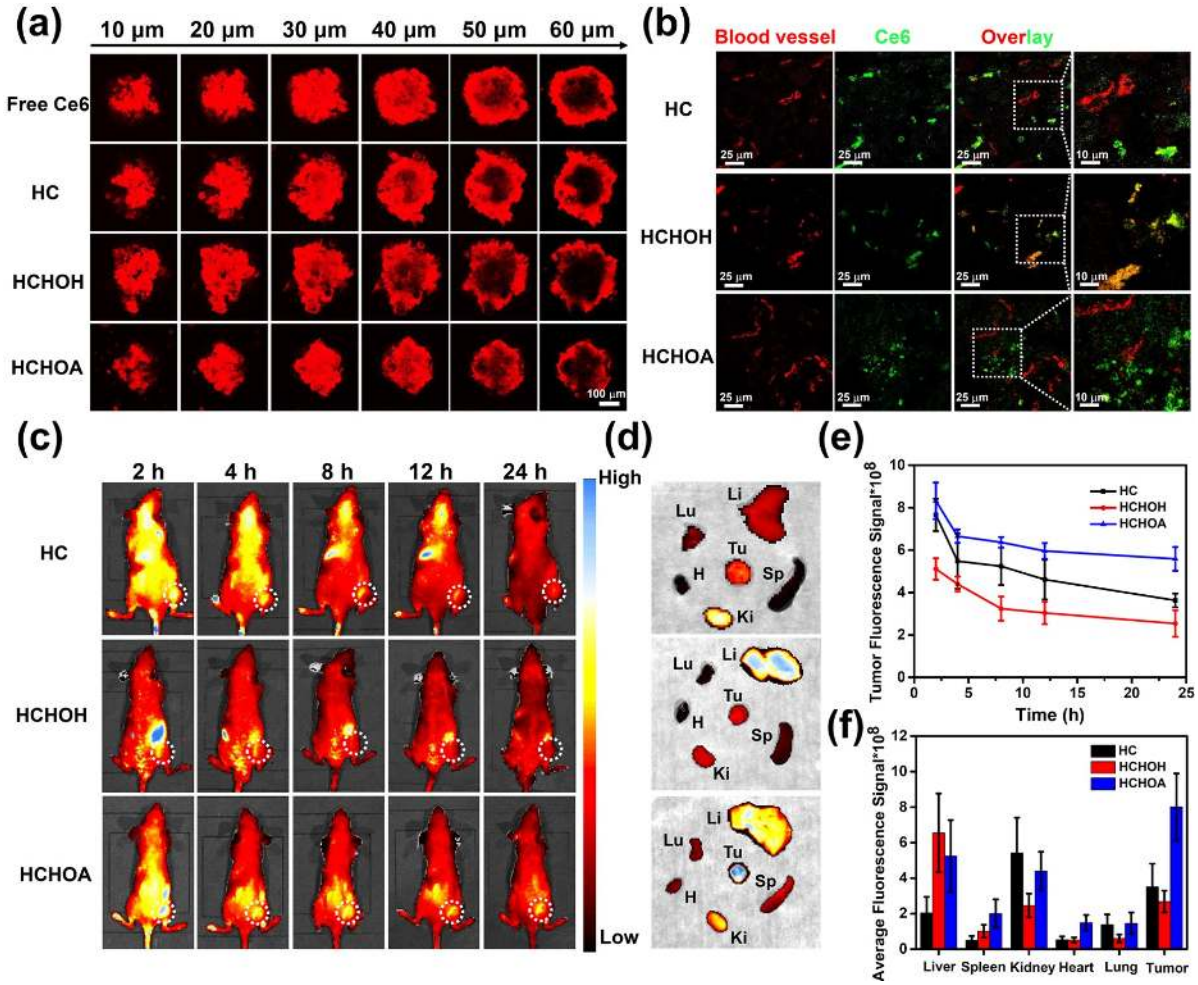

Figure 4. Intratumoral penetration and *in vivo* fluorescence of HCHOA nanoparticles. (a) *In vitro* penetration of Ce6 into MCTSs after the incubation with free Ce6, HC, HCHOH, or HCHOA in hypoxic conditions for 24 h. (b) Confocal fluorescence images of tumor slices from mice at post-24 h injection of HC, HCHOH, or HCHOA. Red and green signals were from the anti-CD31 stained blood vessels and Ce6 fluorescence, respectively. (c) Time-dependent fluorescence images of HC, HCHOH, or HCHOA in mouse models. (d) *Ex vivo* fluorescence images of major organs and tumors taken at 24 h after intravenous injection of HC, HCHOH, or HCHOA nanoparticles. Li, Sp, Ki, H, Lu, and Tu stand for liver, spleen, kidney, heart, lung, and tumor, respectively. (e) Relative fluorescence intensity of tumors from these three groups of mice based on *in vivo* fluorescence images indicated in (c). (f) Semi-quantitative *ex vivo* fluorescence intensity of major organs and tumors in (d).

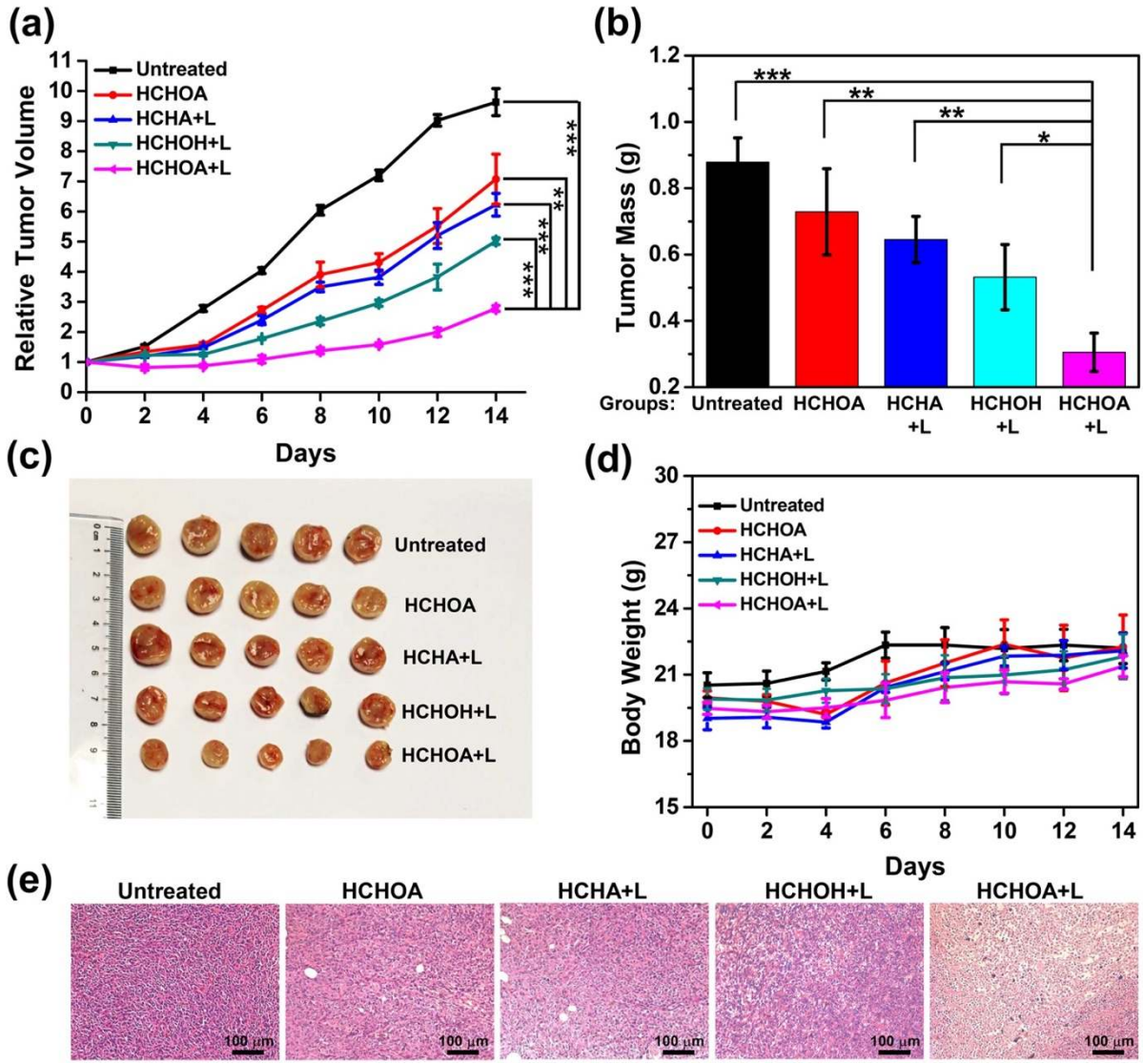

Figure 5. *In vivo* anticancer therapy with HCHOA nanoparticles. (a) Tumor growth curves of different groups after various treatments in 4T1 tumor model. (b) Average tumor weights of mice at the end of different treatments. (c) Photographs of tumors taken from different groups of mice after 14 days. (d) Changes of average body weights from mice after different treatments indicated. (e) H&E stained images of tumor slices taken from different groups at day 5. Error bars from (a) and (d) were based on standard errors of the mean. *p* values in (a) and (b) were calculated by Tukey's post-test (***$p < 0.001$, **$p < 0.01$, or *$p < 0.05$).

TOC Figure

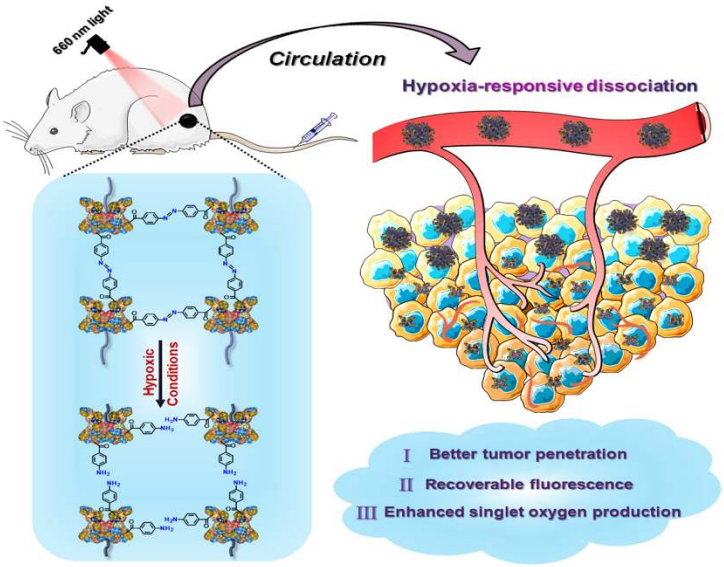

A hypoxia-responsive albumin-based nanosystem could be dissociated into individual therapeutic agents with sizes below 10 nm for increased intratumoral permeability under tumor hypoxic environment. The photoactivity of the loaded chlorin e6 is activated with recovered fluorescence and increased singlet oxygen production, achieving superior antitumor treatment on animal models through combined photodynamic therapy and chemotherapy.